Icarus 237 (2014) 306–314

Contents lists available at ScienceDirect

Icarus

journal homepage: www.elsevier.com/locate/icarus

Time variations of $O_2(a^1\Delta)$ nightglow spots on the Venus nightside and dynamics of the upper mesosphere

Lauriane Soret [a,*], Jean-Claude Gérard [a], Giuseppe Piccioni [b], Pierre Drossart [c]

[a] Laboratoire de Physique Atmosphérique et Planétaire, Université de Liège, Liège, Belgium
[b] IAPS-INAF, Rome, Italy
[c] Observatoire de Paris – Meudon, LESIA, Meudon, France

ARTICLE INFO

Article history:
Received 28 October 2013
Revised 13 February 2014
Accepted 15 March 2014
Available online 26 April 2014

Keywords:
Venus
Venus, atmosphere
Atmospheres, dynamics
Terrestrial planets

ABSTRACT

The dynamical regime of the Venus upper atmosphere is mainly decomposed into three regions. The first one, located below 65 km of altitude is governed by the retrograde superrotational zonal (RSZ) circulation. The second region above 130 km is dominated by the subsolar to antisolar (SS–AS) circulation. The dynamics of the transition region in between are still not fully understood. However, the $O_2(a^1\Delta)$ nightglow emission at 1.27 μm, whose emitting layer is located at ~96 km, can be used as a tracer of the dynamics in this transition region and the imaging spectrometer VIRTIS-M on board Venus Express, orbiting Venus since April 2006, acquired a large amount of nadir observations at this wavelength.

Several previous studies showed that the $O_2(a^1\Delta)$ nightglow emission is statistically located near the antisolar point. In this study, individual VIRTIS-M nadir observations have been analyzed to investigate the variability of the phenomenon. Bright patches of 1.27 μm airglow have been extracted from every observation. It appears that the location of the bright patch is highly variable, even though the brightest patches occur near the antisolar point.

Nadir observations have also been divided into time series, allowing generating animations to follow the intensity and the displacement of bright patches over time. Apparent wind velocities and characteristic decay/rise times and have been deduced from these time series. The speed of the displacements varies from ~0 up to 213 m s^{-1}, with a mean value of 54 m s^{-1}. Owing to the high variability of the direction of the displacements both in the short and the long terms, no clear trend of a global motion at ~96 km can be deduced from these observations. The mean decay time is ~750 min while the mean rise time is ~1550 min. The decay time can be explained as a combination of radiative decay and atomic oxygen transport.

1. Introduction

Our understanding of the Venus atmosphere dynamics has increased only recently, mostly through measurements from the Venera 9 and 10, the Pioneer Venus orbiter, the Galileo flyby and the Venus Express missions. Among others, Bougher et al. (1997, 2006) and Lellouch et al. (1997) reviewed these data sets. A picture of the Venus atmosphere dynamics has emerged. It can mainly be decomposed into three dynamical regions. The first one is characterized by the retrograde superrotational zonal (RSZ) circulation, whose origin is still poorly understood. It starts at ~10 km of altitude (Schubert et al., 1980) and continuously grows up to 65 km where the wind speed can reach ~100 m s^{-1} (Counselman et al., 1979, 1980). This circulation weakens above the cloud top. The second clearly identified region is located above 120 km where the strong temperature gradient between the dayside and the nightside of the Venus upper atmosphere causes a stable subsolar to antisolar (SS–AS) circulation (Schubert et al., 2007). Finally, the region in between (from 70 to 120 km) can be seen as a transition region which is still not fully understood nor quantified. On the Venus nightside, a high degree of variability of the wind velocities has been observed in this transition region. Widemann et al. (2007) performed high-resolution Doppler spectroscopy in $^{12}C^{16}O_2$ visible band (at 74 km) and in solar Fraunhofer lines (at 67 km) on the Venus nightside. They deduced a mean equatorial velocity of ~75 m s^{-1}. No sign of a SS–AS circulation has been observed in this region, confirming that this pattern only occurs at higher altitudes. Clancy et al. (2008, 2012) made Doppler wind profile measurements at 95–115 km on the Venus nightside using sub-millimeter ^{12}CO and ^{13}CO line absorptions. They found out an average

* Corresponding author.
E-mail addresses: Lauriane.Soret@ulg.ac.be (L. Soret), JC.Gerard@ulg.ac.be (J.-C. Gérard), Giuseppe.Piccioni@iaps.inaf.it (G. Piccioni), Pierre.Drossart@obspm.fr (P. Drossart).

http://dx.doi.org/10.1016/j.icarus.2014.03.034
0019-1035/

retrograde zonal wind of 85 m s^{-1} and a SS–AS circulation of 65 m s^{-1} at ~110 km. The variability of these velocity measurements was quite large though. Moullet et al. (2012) made interferometric observations of the CO(1-0) line at the morning terminator. Their model results show that the observed winds on the nightside at 91–108 km are best reproduced when considering a SS–AS flow of 200 m s^{-1} at the terminator and a RSZ wind of 70–100 m s^{-1}. These results were confirmed by Sornig et al. (2013), who made infrared Doppler wind measurements of the CO_2 emission line at 10.5 μm. They observed wind velocities between 41 and 189 m s^{-1} at 110 ± 10 km. However, they attributed these winds to the SS–AS circulation and showed no evidence for a RSZ pattern at these altitudes.

The Venus upper atmosphere dynamics have also been studied by analyzing nightglow emissions. Such emissions occur when atoms carried from the dayside to the nightside by the SS–AS circulation recombine during the gas descent (due to the increasing atmospheric density) to produce a molecule in an excited state that finally emits a radiation when relaxing to its ground state.

Ground-based observations have been performed (Bailey et al., 2008; Ohtsuki et al., 2008) but the Venus Express spacecraft, and especially the VIRTIS (Visible and Infrared Thermal Imaging Spectrometer) and SPICAV (Spectroscopy for Investigation of Characteristics of the Atmosphere of Venus) instruments on its board, highly increased the possibilities to study these emissions. The Venus upper atmospheric dynamics thus appear to be highly complex when considering the averaged morphology of emissions such as the NO and O_2 nightglow. The statistical maximum brightness of the NO nightglow was found to be located at 115 ± 2 km and occurs at 02:00 LT (Stewart et al., 1980; Gérard et al., 2008a; Stiepen et al., 2012, 2013). By contrast, the $O_2(a^1\Delta)$ nightglow, located at 96 ± 2.7 km, occurs near the antisolar point (Gérard et al., 2008b, 2009b; Migliorini et al., 2011; Piccioni et al., 2009; Soret et al., 2012b). The fact that the SS–AS circulation could be prominent at 96 km (the O_2 nightglow being centered at the antisolar point) but not at 115 km (the NO nightglow being shifted toward dawn) is highly unexpected and in contradiction with the global SS–AS circulation previously described (Brecht et al., 2010; Gérard et al., 2009a). Brecht et al. (2011) managed to reproduce this situation with the three-dimensional Venus Thermospheric General Circulation Model (VTGCM). To fit the Venus Express observations, they concluded that between 80 and 110 km, only a weak RSZ flow was needed in addition to a SS–AS circulation of ~40 m s^{-1}. However, at ~95 km, simulated total zonal winds are weak and do not exceed 20 m s^{-1}. Hueso et al. (2008) also tried to better understand this transition region by analyzing individual VIRTIS–Venus Express airglow images acquired at 1.27 μm, mainly during July 2006. They retrieved maps of apparent motions of the $O_2(a^1\Delta)$ nightglow at 95–107 km, which show an extreme variability. This variability was already observed by Crisp et al. (1996) who analyzed the $O_2(a^1\Delta)$ nightglow with ground-based imaging and spectroscopic observations. They showed both extreme spatial and temporal variations of the emission: the brightest regions can vary by more than 20% on time scales of 1 h and disappear in less than a day. Hueso et al. (2008) found zonal velocities ranging from +60 (prograde) to −50 (retrograde) m s^{-1} and meridional velocities ranging from −20 (poleward) to +100 (equatorward) m s^{-1}. The variations of the emission brightness were not studied by Hueso et al. (2008).

In the present study, the entire VIRTIS–Venus Express database has been analyzed. The location and the brightness of the $O_2(a^1\Delta)$ airglow emission on the Venus nightside have been extracted from nadir observations at 1.27 μm. Important results such as apparent wind velocities and characteristic e-folding times have then been deduced from these observations. Section 2 focuses on presenting the VIRTIS nadir observations and the method used to extract information from these measurements. Section 3 describes apparent wind measurements, while Section 4 provides results about the intensity variations of the $O_2(a^1\Delta)$ nightglow emission. Conclusions are discussed in Section 5.

2. Nadir observations and data extraction

2.1. VIRTIS-M statistical results

The European Space Agency (ESA) Venus Express mission was launched on November 9, 2005 and has been orbiting around Venus since April 2006 on a 24-h polar elliptical orbit. The VIRTIS instrument onboard Venus Express is composed of two spectrometers: the VIRTIS-H high-spectral resolution spectrometer and the VIRTIS-M medium-spectral resolution imaging spectrometer (Drossart et al., 2007; Piccioni et al., 2009). VIRTIS-M can be used in the visible/NIR channel from 0.3 to 1 μm by steps of ~2 nm or in the IR channel from 1 to 5 μm by steps of ~10 nm. The VIRTIS-M-IR instrument is well adapted to the observation of the $O_2(a^1\Delta)$ nightglow at 1.27 μm either in nadir or limb modes. A VIRTIS-M-IR observation typically lasts 20 min. Due to the quasi-polar elliptical orbit of Venus Express, whose apocenter is located 66,000 km away from Venus South pole, the nadir mode is used when observing the southern hemisphere of the planet, while limb observations are preferentially made when looking at the northern hemisphere. With its 64 mrad field of view, a VIRTIS-M-IR nadir observation cannot reveal more than 25% of the Venus nightside when the spacecraft is near apocenter. Based on VIRTIS-M nadir observations corrected from geometrical effects and thermal emission, Gérard et al. (2008b) and Piccioni et al. (2009) found that the emission peak is statistically located around the antisolar point, with an averaged maximum value of respectively 3 MR and 1.2 MR (1 Rayleigh, *R*, corresponds to the brightness of an extended source emitting 10^6 photons cm^{-2} s^{-1} in 4π sr) and a mean intensity for the Venus nightside of 1.3 MR and 0.52 MR, respectively. Averaging nadir and limb data from the entire VIRTIS-M-IR database (April 2006–October 2008), Soret et al. (2012a) produced a detailed statistical map of the $O_2(a^1\Delta)$ nightglow emission. They corrected the nadir observations for the thermal contribution originating from hot regions of the surface and lower atmosphere. To do so, they removed 30% of the thermal emission observed in the bands 1.14–1.21 μm from the raw $O_2(a^1\Delta)$ emission, which spread from 1.23 to 1.30 μm (Cardesin-Moinelo, 2009; Piccioni et al., 2009). Data were also corrected for emission angle and backscattering following the method developed by Crisp et al. (1996). Then, they added all the individual VIRTIS-M-IR data projected on a grid and divided this global map by a map of the number of contributions per bin. Fig. 1a shows a similar binned map (bins of 15 min × 1°) of the averaged $O_2(a^1\Delta)$ nightglow emission in a cylindrical projection based on 3174 nadir observations. The number of image contributions per map bin can be seen in Fig. 1b. Near the South pole, up to 360 observations/bin contribute to the estimation of the mean 1.27 μm brightness. Fig. 1a shows an enhanced emission around the antisolar point, with a maximum brightness of 2.1 MR. The hemispheric mean vertical brightness on the Venus nightside is 0.50 MR. Fig. 1c represents a binned map of the brightness standard deviation. It shows the same morphology as Fig. 1a. The variability is very weak in the Southern hemisphere. The highest values of the brightness standard deviation occur near the antisolar point, where it reaches 1.3 MR. This already suggests a high variability of the emission in this area. The global mean standard deviation is 0.29 MR.

All the statistical observations from Gérard et al. (2008b), Piccioni et al. (2009) and Soret et al. (2012a) tend to confirm the dynamical–chemical scheme initially proposed by Connes et al.

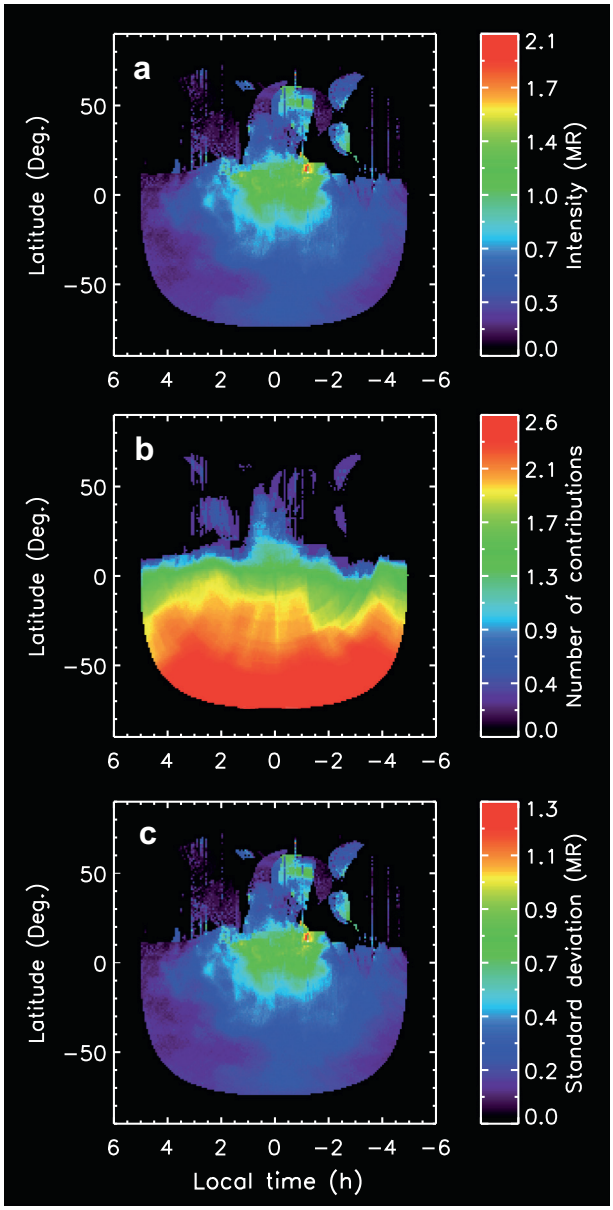

Fig. 1. (a) Statistical map of the $O_2(a^1\Delta)$ nightglow generated with nadir VIRTIS-M observations. (b) Number of contributions per map bin used to generate (a). (c) Brightness standard deviation associated to (a).

(1979). They suggested that the observed emission at the antisolar point corresponds to radiative relaxation of metastable $O_2(a^1\Delta)$ molecules following three-body recombination of oxygen atoms descending in the atmosphere. These atoms are produced on the Venus dayside by photodissociation and electron impact dissociation of CO_2 and CO and transported to the nightside by the subsolar to antisolar (SS–AS) circulation. The reaction scheme may be written:

$$2O + CO_2 \rightarrow O_2(a^1\Delta) + CO_2 \quad (1)$$

$$O_2(a^1\Delta) \rightarrow O_2 + h\nu\ (1.27\ \mu m) \quad (2)$$

$$O_2(a^1\Delta) + CO_2 \rightarrow O_2 + CO_2 \quad (3)$$

However, it is important to point out that the $O_2(a^1\Delta)$ emission is located only statistically at the antisolar point following accumulation of all the 3174 nadir data collected by VIRTIS-M-IR. This is best demonstrated by considering sets of 500 observations at a time. Binned maps of Fig. 2 show that the mean bright emission patch is not always located at the antisolar point and that the maximum nadir intensity can vary from 2.3 to 3.3 MR. The coverage for the generation of each map is yet quite similar, with a coverage morphology identical to Fig. 1b and up to 231 nadir observation contributions per map bin (with a mean of 65 contributions per bin). Fig. 2a shows indeed that the average of the 500 first VIRTIS-M nadir observations reveal a bright emission spot located around the antisolar point, from 23:00 to 01:00 LT and 25°S to 10°N, with a maximum brightness of 2.7 MR. Fig. 2b shows that the assembly of the next 500 VIRTIS-M nadir observations also creates an extended patch around the antisolar point, but its morphology is quite different and less intense (~1.4 MR). Fig. 2c suggests that the bright patch is once again located where it is expected to occur if it is controlled by the SS–AS circulation. Fig. 2d is however more complex. Three patches can be observed: one at ~23:00 LT – 10°N, a second one at ~01:30 LT – 5°N and, finally, the last one is centered at ~03:00 LT – 10°S, which is quite distant from the antisolar point. Fig. 2e shows a main bright patch of ~1.6 MR at ~01:00 LT – 5°S. Even though Fig. 2f shows an enhanced region of 1.3 MR from 21:00 to 02:00 LT and from 15°S to 15°N, two even brighter spots appear at ~22:00 LT – 0°. This partial statistical map is thus highly asymmetrical. Finally, the bright spot observed in Fig. 2g (generated with the remaining 174 VIRTIS-M-IR nadir observations) is also shifted toward dusk, at ~22:30 LT – 0°. All these asymmetries associated to a limited sample of nadir observations cause what could be seen as several red and yellow patches in Fig. 1a but is, in reality, no more than a statistical artifact of the high variability of the circulation in the transition region over time. The situation becomes even more complex when looking at individual VIRTIS-M nadir observations rather than statistical maps. This point is examined in further details in the following section.

2.2. Individual VIRTIS nadir observations

In this study, all the 2465 $O_2(a^1\Delta)$ VIRTIS-M nadir observations have been processed the way described by Soret et al. (2012a). However, data have not been added together to generate a global map, but individually projected on a Venus nightside grid and checked to remove those showing a poor resolution and/or a poor coverage of the Venus nightside. Some examples of usable individual nadir observations are illustrated in Fig. 3 (bins are 15 min × 1°). They show that, owing to the small angular aperture of VIRTIS, it is never possible to observe the full Venus nightside with a single observation. They also clearly demonstrate that the bright $O_2(a^1\Delta)$ emission patches are not always located at the antisolar point. These patches occasionally appear at very high latitudes, near the southern pole (no nadir data are available for the northern hemisphere, as previously mentioned).

Fig. 3a–c were acquired at very different times (9 July 2006, 22 February 2007 and 26 April 2007, respectively). However, nadir observations can also be grouped in order to generate series of consecutive images pointing at the same Venus nightside region over a limited period of time. The area covered by each frame varies with time as a result of the spacecraft motion toward the planet during each observation sequence. A total of 214 time series have been generated, allowing to follow the evolution of bright emission patches. Fig. 4a–d illustrate one of them. It was acquired on 9 July 2006, from 16:10 to 19:30 UT during orbit 80. The change in the intensity of the emission is obvious but the displacement of the patch is not. These variations can however easily be observed when looking at Animation 1. In Animation 1, the four images of Fig. 4a–d have been put in sequence and a fixed white star symbol marks the location of the brightest patch bin in the first image of the sequence. The patch displacement toward dusk is obvious

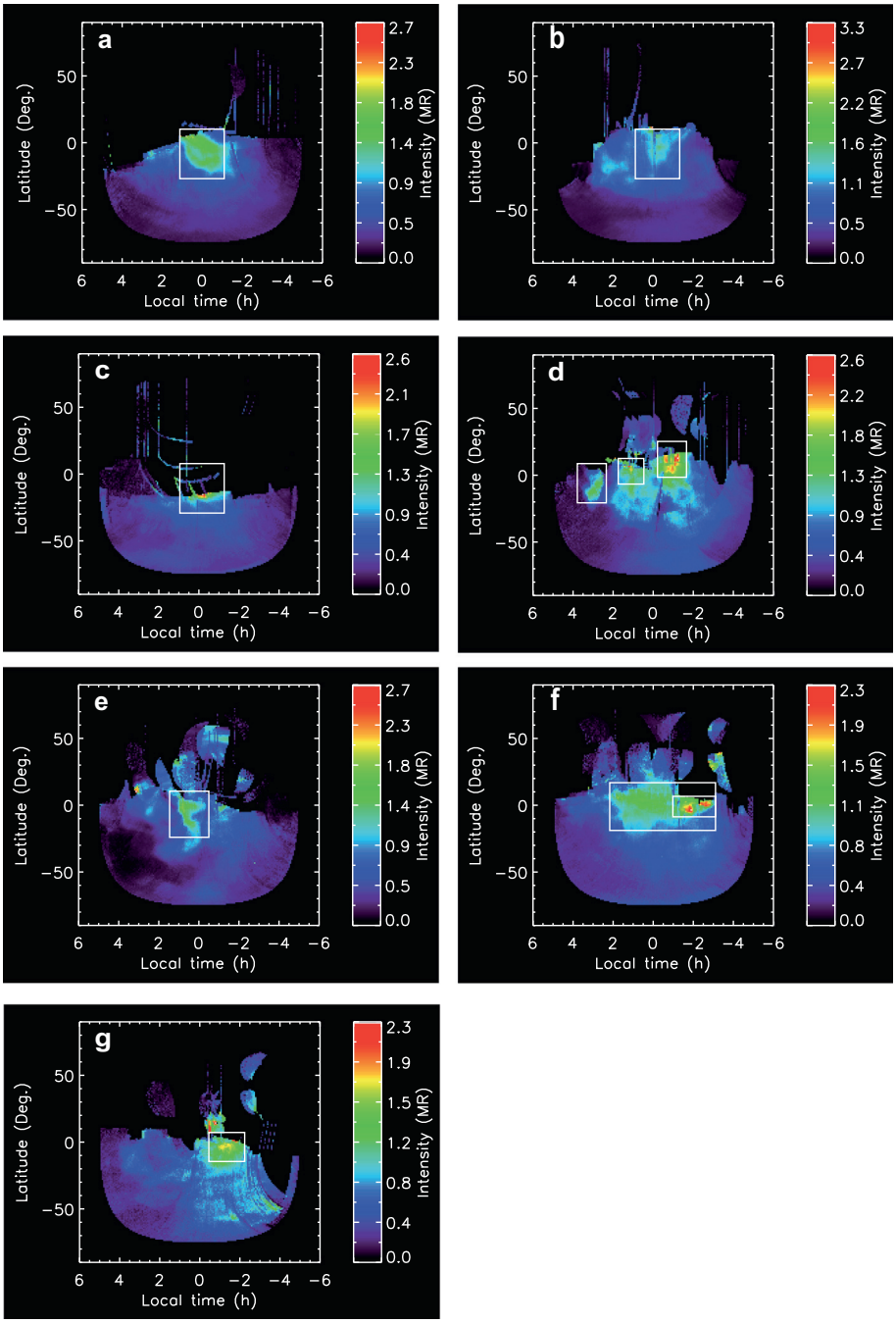

Fig. 2. Fragmentation of the data represented in Fig. 1a in nadir observations acquired between May 14, 2006 and August 9, 2006 (a), August 9, 2006 and September 16, 2006 (b), September 16, 2006 and February 13, 2007 (c), February 13, 2007 and April 26, 2007 (d), April 26, 2007 and November 6, 2007 (e), November 6, 2007 and July 1st, 2008 (f) and between July 5, 2008 and October 15, 2008 (g). Regions of bright emission are enhanced with white boxes.

and so is its brightness increase during the first three observations, then followed by a decrease from ~2.3 MR to 1.7 MR in the last image (3 h after the first one). Animations 2–5 have also been generated in order to show other examples of time series. Animation 2 refers to orbit VI0308 (already shown in Fig. 3b). In this case, three main patches can be observed. The brightness of one of them (marked with a white star symbol) keeps increasing while the other two decrease. This result shows a great variability of the emission within a single sequence in a 4-h period of time. The main displacement is directed toward North. In Animation 3 (orbit VI0371, already shown in Fig. 3c), no significant displacement can be observed. The bright patch intensity increases in 5 h from ~1.8 MR to 4.5 MR. In Animation 4 (orbit VI0324), four patches can be observed at the beginning of the series, all moving northward. The brightness of only one of them clearly increases from ~1.1 to 2.2 MR in 5 h. Finally, three main patches can also be observed during 5 h in Animation 5 (orbit VI0367). Two of them move southward while the southernmost (~35°S) one heads toward dusk and South. Note that, in some images, nadir observations appear rougher as a consequence of shorter exposure times and lower signal to noise ratios.

In order to properly analyze the database, only series showing patches far enough from the edges of the field of view have been selected. A total of 127 images, distributed among 47 time series

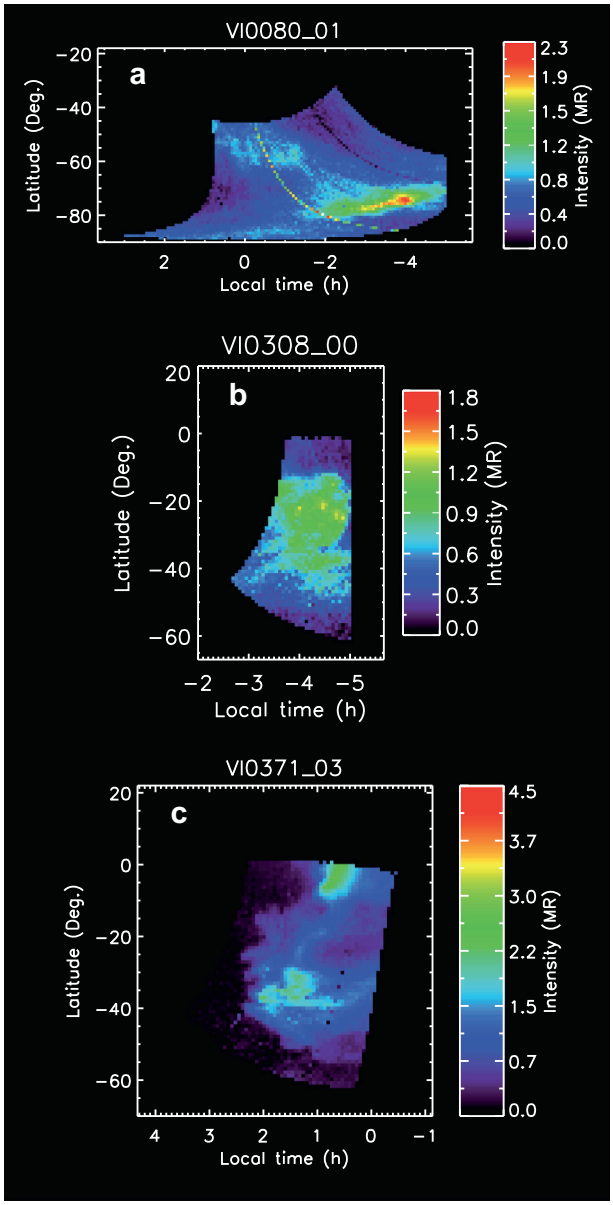

Fig. 3. Examples of individual nadir observations of the $O_2(a^1\Delta)$ airglow structure. A VIRTIS-M-IR nadir observation cannot cover more than 25% of the Venus nightside. The bright emission patch can be located away from the antisolar point.

of observations were finally used for this study. These time series, from the first to the last nadir observation of the series, can last from 45 to 3200 min. Note that, occasionally, several patches can be observed in a given time sequence (see Animations 2, 4 and 5). These images have then been processed with a blob-coloring technique in order to automatically extract the brightest patch from the image. The blob-coloring technique consists in applying a threshold to an individual image so it becomes a binary image. An 8-connexity filter is then applied to check whether a given bin belongs to one group of bins or another. The brightest group of bins finally corresponds to the emission patch. Fig. 4a–d patches extraction can be seen in Fig. 4e–h, respectively. The coordinates (latitude and local time) of the patch barycenter have been estimated and associated to the averaged intensity of the patch. Along with the UT acquisition time of the barycenter, these parameters have then been used to follow the time evolution of the emission patches, both in terms of displacements and intensity. Results are independently presented in Sections 3 and 4, respectively.

3. Apparent wind velocity measurements

The location of the patch barycenter can be followed over time, leading to feature tracking. The red curve in Fig. 5a shows the example of the displacement through the Venus nightside of the bright patch shown in Fig. 4 and Animation 1. In this case, the motion is quite linear, with the spot moving from 71°S to 68°S and between 20:40 and 20:13 LT. For a series of N consecutive images, $N-1$ apparent wind vectors can be retrieved. From the four consecutive images of Fig. 4a–d, three wind vectors have been deduced. The retrieved displacements correspond to apparent motions of 22.7, 42.0 and 45.8 m s^{-1}. In other cases, the motion can however be highly random as for example in Fig. 5a in black (VI0364). The associated apparent wind velocities are 44, 25, 119, 177 and 48 m s^{-1}. Considering the 47 generated nadir time series, a histogram of the norms of the wind vector has been plotted (Fig. 6). It shows that the velocity associated with the displacements vary between ~0 up to 213 m s^{-1}, with a mean value of 54 m s^{-1} and a median value of 44 m s^{-1}. Data indicate that most of the velocities range between 5 and 65 m s^{-1}, with only few measurements showing a velocity greater than 120 m s^{-1}. Considering the brightest bin of the emission patch instead of its barycenter leads to an averaged apparent wind velocity of 104 m s^{-1}. Taking into account the apparent wind direction, it appears that the meridional component can reach extreme values of −191 (poleward) to +168 (equatorward) m s^{-1}. The mean poleward value is −37 m s^{-1} and the mean equatorward value is +37 m s^{-1}. Zonal wind velocities range between −177 (retrograde, from dusk to dawn) and +156 (prograde) m s^{-1}, with mean values of −32.3 and +32.8 m s^{-1}, respectively. There is thus no prevailing wind. However, there are as many positive as negative components in the morning and in the evening side, which does not allow concluding for a pure SS–AS circulation. These results are in agreement with those from Clancy et al. (2012) and Sornig et al. (2013) who both observed a very large variability in their measurements. Clancy et al. (2012) found average wind speeds of 65 m s^{-1} and an extremely variable additional zonal component of ~85 m s^{-1}. With their method, Sornig et al. (2013) measured speed values between 41 and 189 m s^{-1}, but did not find any evidence for a global RSZ component. Brecht et al. (2011) modeled wind speeds of the same order with the VTGCM. They showed that zonal winds are less than 20 m s^{-1} at 95 km. They stressed the fact that their three-dimensional model gives averaged steady state values that cannot reproduce the variability of the observations.

Apparent wind vectors are shown in Fig. 7: the displacements appear to be highly random both in norm and direction. For example, the region at ~03:00 LT and 10°S shows that some vectors (belonging to the same series) point toward the northern direction, but others (belonging to another series) point toward dawn, implying that the wind direction in a given region may significantly vary over time. Thus, as mentioned before, the VIRTIS-M observations provide a totally new view of the circulation variability. As a matter of fact, all previous studies were based on relatively short acquisition times (~10 min for Sornig et al. (2013) and 2–15 min for Clancy et al. (2012)) but consecutive observations were separated from several days or months. Also, the number of observations was highly limited. By contrast, in this study, even though acquisition times are longer (~20 min are necessary to obtain a VIRTIS observation, which could somewhat smooth the very short-term variability of the phenomenon), consecutive observations are separated by less than an hour and the VIRTIS database covers more than two years of observations. It is thus possible to observe the variability of the $O_2(a^1\Delta)$ emission on both the short term (every 20 min) and the long-term (from April 2006 to October 2008). Animation 2 goes even further

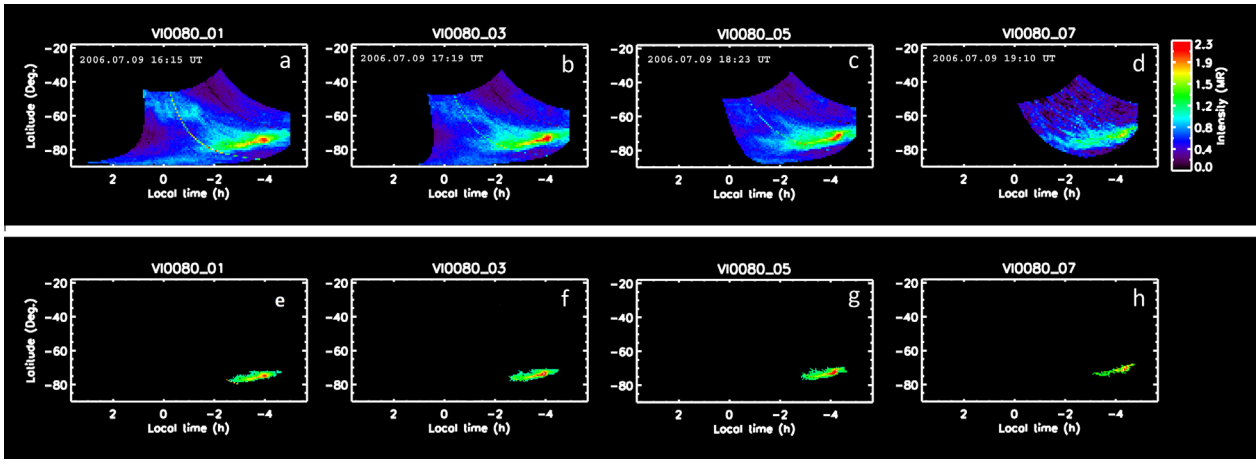

Fig. 4. Example of a time series (a–d) where a bright $O_2(a^1\Delta)$ patch can be observed. It has been extracted (e–h) from the VIRTIS-M nadir observations (a–d, respectively) using a blob-coloring algorithm. (For interpretation of the references to color in this figure legend, the reader is referred to the web version of this article.)

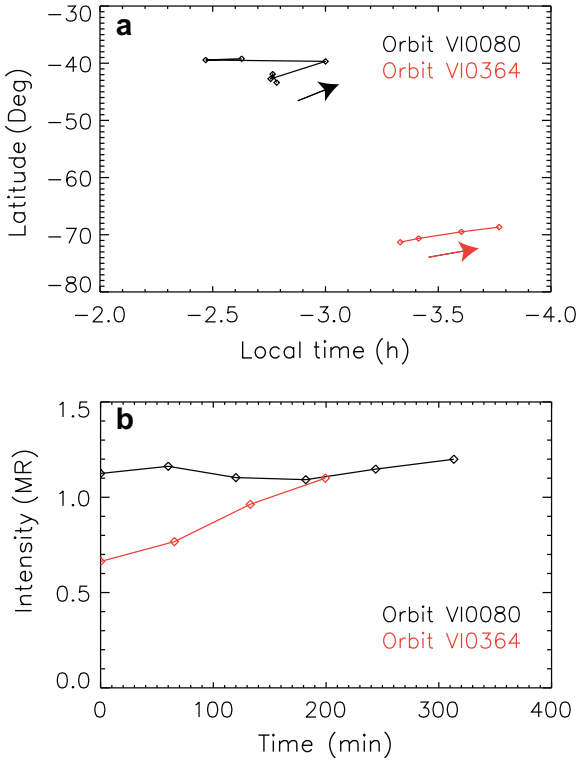

Fig. 5. The displacement the bright patch emission shown in Fig. 4 (orbit 80) is represented (a in red) and its intensity is plotted against time (b in red). Another example of a series acquired on April 19, 2007 (orbit 364) is represented in black. (For interpretation of the references to color in this figure legend, the reader is referred to the web version of this article.)

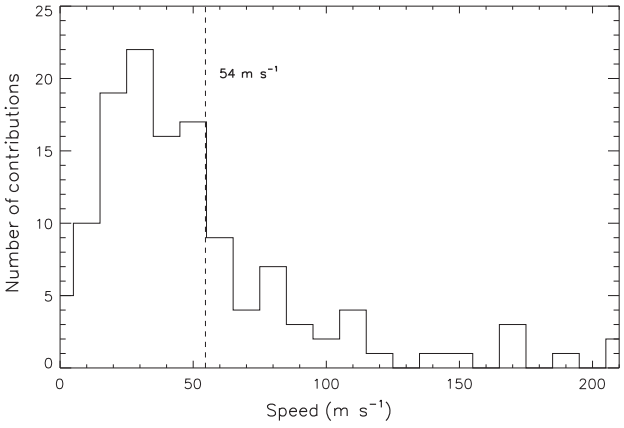

Fig. 6. Histogram of the apparent wind speed deduced from 127 nadir VIRTIS-M observations. The velocity of the displacements varies between ~0 up to 213 m s^{-1}, with a mean value of 54 m s^{-1}.

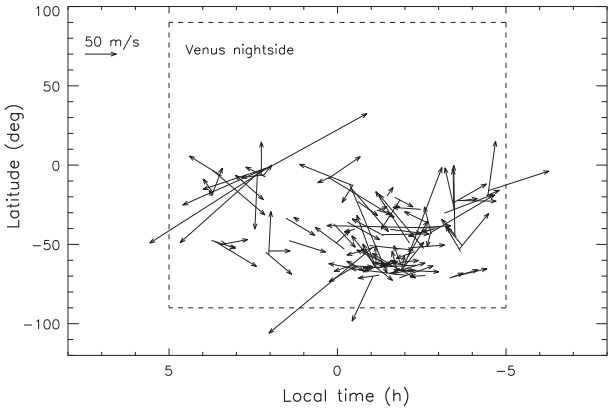

Fig. 7. Map of the apparent wind vectors measured on the Venus nightside (dashed area). The plot shows that winds are highly variable in space and time and may reach up to 213 m s^{-1}.

in the variability of the emission by showing several patches evolving differently in orbit 308: some patches increase while other decrease and the bright patch located at ~20:50 LT – 25°S moves northward while the area at ~20:30 LT – 37°S moves southward.

Hueso et al. (2008) previously generated maps of apparent wind velocities but they used a restricted sample of VIRTIS-M nadir observations. They determined a global circulation on the Venus nightside (Fig. 5 from Hueso et al., 2008). From 0 to ~30°S, the global trend is directed from dawn to dusk (prograde). A rotating motion can be observed near 22:00 LT – 50°S. They found apparent zonal velocities ranging between +60 (prograde) and −50 (retrograde) m s^{-1} and apparent meridional velocities from −20 (poleward) to +100 m s^{-1} (equatorward) with an average meridional circulation of +20 m s^{-1} toward low latitudes. Based on the highly

inhomogeneous apparent wind vectors shown in Fig. 7 and contrary to Hueso et al. (2008), no significant global motion pattern at 96 km can been deduced from this study. In particular, these vectors do not appear to reproduce either a RSZ or a SS–AS circulation. This result is reminiscent of the study by Bougher et al. (2006) who observed a large spatial and temporal variability in the distribution of the individual bright airglow patches of nitric oxide airglow over 24-h periods with the UVS instrument on board Pioneer Venus. They concluded to a highly variable day-to-day thermospheric circulation.

Both our wind study and that from Hueso et al. (2008) have been made without considering the brightness evolution of the $O_2(a^1\Delta)$ patch. This is quite important though, as the apparent displacement might not always represent an actual wind speed but can also stem from a change in the global circulation or variations in the local vertical transport efficiency on the nightside. Intensity variations, independently from dynamical motions, will be discussed in the following section. Either way, this study of apparent displacements characterizes the dynamical behavior in the Venus upper mesosphere at ~96 km and confirms its high variability both a short- and long-terms.

4. Intensity variations

This section will focus on analyzing the intensity variations of the emission, independently from the patch displacement. Contrary to Section 3, where the patch barycenter was used to deduce the global motion of the $O_2(a^1\Delta)$ emission, this section uses the brightest bin of the extracted patch. Using the barycenter and an averaged brightness smoothes the data and no proper analysis would have been possible.

4.1. Spatial intensity variations

First, the coordinates of the emission maximum for each of the 127 selected nadir observations have been plotted similarly to the example in Fig. 8. An important result readily appears: the location of the emission patch is highly variable. Bright emission patches have been observed in almost any region of the Venus nightside covered by nadir observations (Southern hemisphere, from 19:00 to 05:00 LT). A color code has also been assigned to each point of Fig. 8, depending on the intensity of the observed patch. The color bar shows that the intensity maximum is also highly variable, ranging from very low to more than 3 MR, with a mean value of 1.75 MR. The concentration of red dots around the antisolar point is consistent with the results showed in Fig. 1: bright $O_2(a^1\Delta)$ emissions can occur everywhere, but the brightest ones statistically occur in the vicinity of the antisolar point. The addition of a large number of individual observations makes the global pattern emerge. As mentioned before, it is important to note that a VIRTIS-M nadir observation never covers the entire Venus nightside. Thus, a bright patch detected near the South pole does not prevent an even brighter emission from occurring at the antisolar point at the exact same time. This can easily be observed when examining Fig. 5d of Piccioni et al. (2009). This VIRTIS-M limb observation shows that a bright spot can occur at 30°N while another one is seen near the equator. Gérard et al. (2014) also present several VIRTIS-M-IR limb images of the $O_2(a^1\Delta)$ emission. In most examples, several patches can be observed along latitudinal cuts.

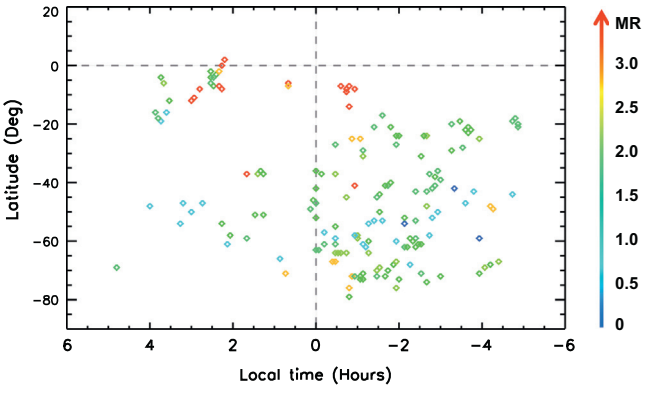

Fig. 8. Dots represent the position of the emission maximum on the Venus nightside extracted from 127 nadir VIRTIS-M images. The dot color corresponds to the intensity of the emission. It shows that the $O_2(a^1\Delta)$ emission is highly variable both in location and intensity.

4.2. Temporal intensity variations

The variations of the bright patch intensity of each series of nadir observations have also been followed over time. Both intensity increases and decays have been observed during the time series. Fig. 5b is an example of a bright patch weakening. Altogether, out of the 47 generated series, 20 of them show a decrease of the intensity, 16 present an increase (Animation 3) and the other 11 exhibit both increases and decreases over time (Animation 1 and Fig. 5b in black). They are randomly distributed over space and time. The intensity drops are expected as a direct consequence of the long radiative lifetime of ~75 min of the $O_2(a^1\Delta)$ metastable state and the recombination of the O atoms producing this excited state though process (1). As for the increasing phases, they can probably be explained by a continuous supply of fresh oxygen atoms provided by the SS–AS circulation which recombine while producing $O_2(a^1\Delta)$ molecules. These assumptions need to be verified in the next section by considering the characteristic times of the intensity variations.

4.3. E-folding times

In this work, for simplicity, we assume that the intensity decreases (increases) follow an exponential law:

$$I(t) = I_0 \cdot e^{(-\Delta t/\tau)} \quad (4)$$

where I is the intensity, I_0 is the intensity at the beginning of the series, t is the time, and τ is the effective decay (rise) time. These e-folding times have been estimated for every series of nadir observations. Decay times range from 72 to 2715 min, with a mean value of ~750 min. The mean rise time is ~1550 min. The mean decay time is thus ten times longer than the oxygen atoms radiative lifetime of 75 min. Therefore, in most cases, radiative processes alone cannot explain the intensity decay observed in the Venus atmosphere. This apparent inconsistency can however be solved when considering the chemical lifetime of the atomic oxygen atoms which continuously produce $O_2(a^1\Delta)$ molecules together with the vertical transport time scales. The rate of the O_2 airglow decay actually depends on the atomic oxygen density in the upper mesosphere, as the effective chemical lifetime of O atoms in the upper mesosphere, equal to $\tau_O = 1/k[O][CO_2]$, controls the production of the $O_2(a^1\Delta)$ through reaction (1). We use the one-dimensional chemical-diffusive atmospheric model developed by Gérard et al. (2008a), together with the hemispheric mean O and CO_2 density profiles determined by Soret et al. (2012b) based on VIRTIS and SPICAV data, to quantify the chemical lifetimes τ_O and $\tau_{O_2(a^1\Delta)}$, the molecular diffusion time scale τ_D and the eddy diffusion time scale τ_K. Their vertical distribution can be seen in Fig. 9. The effective lifetime of $O_2(a^1\Delta)$ molecules remains equal to its radiative value down to about 90 km, where quenching by CO_2 starts decreasing its value. The calculated chemical lifetime of atomic oxygen is on the order of

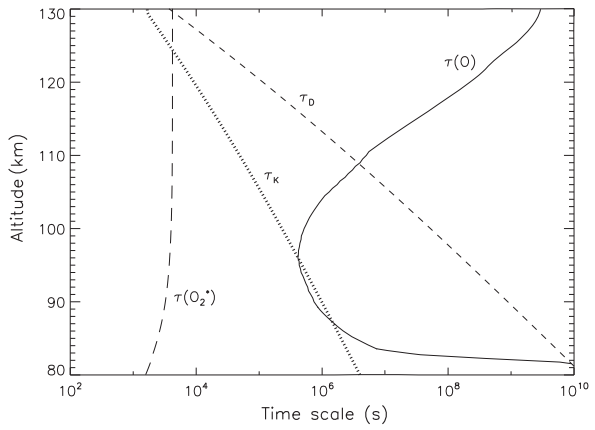

Fig. 9. Time scales calculated with the one-dimensional chemical-diffusive atmospheric model by Gérard et al. (2008a), using the hemispheric mean O and CO_2 density profiles based on VIRTIS and SPICAV data determined by Soret et al. (2012a). The chemical lifetimes of O and $O_2(a^1\Delta)$ are represented in solid and long-dashed lines, respectively. The molecular diffusion time scale τ_D is plotted in short-dashed line and the eddy diffusion time scale τ_K is represented with a dotted line.

115 h at 96 km, considerably longer than the 75 min of the $O_2(a^1\Delta)$ radiative lifetime. Thus, even though the local supply of O atoms from above is suddenly turned off, local oxygen atoms will continue to recombine with an e-folding value equal to τ_O. Fig. 9 also shows that eddy diffusion plays an important role in the production of the $O_2(a^1\Delta)$ through the control of the O atom vertical distribution. At 96 km, $\tau_K = \tau_O$, which means that the corresponding vertical wind is on the order of $w = H/\tau_K = 1.25$ cm s^{-1} (with $H \approx 5$ km the scale height of $O_2(a^1\Delta)$). The effective decay time of the 1.27 μm airglow is thus a combination of the radiative lifetime of $O_2(a^1\Delta)$ molecules with the O chemical lifetime τ_O and its vertical transport efficiency.

Rise times can easily be explained by an additional downward flux of oxygen atoms, leading to the formation of excited oxygen molecules by three-recombination and an enhanced emission at 1.27 μm during their deactivation.

Changes in intensity could also be caused by a change of altitude of the emission layer. Emissions are indeed expected to be brighter at ~96 km, but weaker above (three-body recombination less efficient) or below (quenching by CO_2) this altitude.

5. Conclusions

This study confirms results obtained in previous works showing that the $O_2(a^1\Delta)$ nightglow emission is highly variable. However, this study brings new insights in that the available VIRTIS-M dataset enabled us to study the $O_2(a^1\Delta)$ emission variations both at the long (years) and short (minutes) terms.

The long term was studied with the statistical results of Section 2. We showed that bright $O_2(a^1\Delta)$ patches can occur in any region of the Venus nightside. However, the bright patch observed in a single observation is not necessarily the brightest patch of the Venus nightside. Indeed, a VIRTIS-M observation cannot cover the entire Venus nightside at once, most of the time avoiding the antisolar region: the brightest emission patch can thus actually be located outside the VIRTIS-M field of view. Despite this bias, the brightest patches tend to statistically occur around the antisolar point. This probably explains why the brightest area of previous airglow statistical maps is located at the antisolar point (Gérard et al., 2008b; Piccioni et al., 2009; Soret et al., 2012a).

Short-term analysis, based on the study of consecutive nadir images, lead to the retrieval of apparent wind velocities and intensity variations. Horizontal winds time scales can also be estimated. Assuming a mean horizontal velocity of 54 m s^{-1} at 96 km (Fig. 6) and the full displacement of a typical size of the bright patch of 1000 km, the calculated horizontal wind time scale is about 2×10^4 s. According to Fig. 9, this time scale is shorter than $\tau_{O_2(a^1\Delta)}$, $\tau_{O_2(a^1\Delta)}$, τ_K and τ_D. Therefore, even though the $O_2(a^1\Delta)$ emission is subject to radiative decay and vertical transport, the dominant cause of all the $O_2(a^1\Delta)$ patch changes is horizontal transport.

Wind speeds at ~96 km have been estimated by following motion of the bright patches over time. The apparent speed was found to vary from ~0 to 213 m s^{-1}, with a mean value of 54 m s^{-1}. A map of the deduced wind vectors has been generated. It shows a high variability for both the short and the long terms: wind vectors deduced from a given time series can change directions and so can the wind vectors of a given region retrieved several orbits later. Apparent zonal and meridional components vary from −177 (retrograde) to +156 (prograde) m s^{-1} and −191 (poleward) to +168 (equatorward) m s^{-1}, respectively, but globally cancel out. These wind velocities are in good agreement with previous studies based on measurements of Doppler shift which also observed a high variability and motions much more complex than a simple SS–AS circulation. It is however challenging to exactly quantify the Venus winds at these altitudes as long as snapshot global views of the airglow distribution are not available.

Intensity variations over time periods of tens of minutes to hours have also been studied. Both increases and decays of the $O_2(a^1\Delta)$ intensity have been observed. Increasing phases can be explained by a local additional supply of oxygen atoms from the dayside. Collet et al. (2010) developed a two-dimensional chemical-transport time dependent model of four minor species in the Venus upper atmosphere. They modeled the spatio-temporal distribution of both the NO and $O_2(a^1\Delta)$ nightglows. They showed that locally enhanced downward fluxes of oxygen and nitrogen increase the brightness of both emissions several hours after the injections and that both the retrieved intensities and e-folding times are highly dependent on the flux values and the duration of the injections. On the other hand, the long decay time (exceeding the 75 min $O_2(a^1\Delta)$ radiative lifetime) can be interpreted as a combination of the radiative decay of the $O_2(a^1\Delta)$ metastable state and the lifetime of the O atoms. Bougher et al. (2006) and Hueso et al. (2008) suggested that the changing intensity distribution on the nightside can also be due to local variations in the atmospheric global circulation (gravity waves or eddy-diffusion coefficient modifications). Allen et al. (1992), Crisp et al. (1996) and Gérard et al. (2014) suggested that these local variations of the nightglow emission could be a consequence of spatial inhomogeneity of the efficiency of vertical transport.

The bright patches followed in this study sometimes change both in intensity and shape. In these cases, (i) oxygen atoms within a given patch may not subject to a uniform motion or (ii) it is also possible that the $O_2(a^1\Delta)$ intensity variations results from a combination of changes in the downward fluxes of oxygen atoms or atmospheric density, or (iii) the presence of gravity waves can modifying the strength of the local vertical transport.

Acknowledgments

We gratefully thank all members of the ESA Venus Express project and of the VIRTIS scientific and technical teams. This research was supported by the PRODEX program managed by the European Space Agency with the help of the Belgian Federal Space Science Policy Office. This work was also funded by Agenzia Spaziale Italiana and the Centre National d'Etudes Spatiales.

Appendix A. Supplementary material

Supplementary data associated with this article can be found, in the online version, at http://dx.doi.org/10.1016/j.icarus.2014.03.034.

References

Allen, D., Crisp, D., Meadows, V., 1992. Variable oxygen airglow on Venus as a probe of atmospheric dynamics. Nature 359, 516–519. http://dx.doi.org/10.1038/359516a0.

Bailey, J., Meadows, V.S., Chamberlain, S., Crisp, D., 2008. The temperature of the Venus mesosphere from $O_2(a^1\Delta_g)$ airglow observations. Icarus 197, 247–249. http://dx.doi.org/10.1016/j.icarus.2008.04.007.

Bougher, S., Alexander, M., Mayr, H., 1997. Upper atmosphere dynamics: Global circulation and gravity waves. Venus II 2, 259–292.

Bougher, S.W., Rafkin, S., Drossart, P., 2006. Dynamics of the Venus upper atmosphere: Outstanding problems and new constraints expected from Venus Express. Planet. Space Sci. 54, 1371–1380. http://dx.doi.org/10.1016/j.pss.2006.04.023.

Brecht, A., Bougher, S.W., Parkinson, C.D., Rafkin, S., Gérard, J.-C., 2010. Concurrent observations of the ultraviolet NO and infrared O_2 nightglow emissions: Uncorrelated behavior explained with the VTGCM. In: International Venus Conference, Aussois, p. 95.

Brecht, A.S., Bougher, S.W., Gérard, J.C., Parkinson, C.D., Rafkin, S., Foster, B., 2011. Understanding the variability of nightside temperatures, NO UV and O_2 IR nightglow emissions in the Venus upper atmosphere. J. Geophys. Res. 116, E08004. http://dx.doi.org/10.1029/2010je003770.

Cardesin-Moinelo, A., 2009. Studio ed implement azione della pipeline dei dati dello spettrometro ad immagini VIRTIS a bordo della mission Venus Express: "Dalla planificazione scientifica delle operazioni fino all'archiviazione dei dati ed all'elaborazione ad alto livello".

Clancy, R.T., Sandor, B.J., Moriarty-Schieven, G.H., 2008. Venus upper atmospheric CO, temperature, and winds across the afternoon/evening terminator from June 2007 JCMT sub-millimeter line observations. Planet. Space Sci. 56, 1344–1354. http://dx.doi.org/10.1016/j.pss.2008.05.007.

Clancy, R.T., Sandor, B.J., Moriarty-Schieven, G., 2012. Circulation of the Venus upper mesosphere/lower thermosphere: Doppler wind measurements from 2001–2009 inferior conjunction, sub-millimeter CO absorption line observations. Icarus 217, 794–812. http://dx.doi.org/10.1016/j.icarus.2011.05.021.

Collet, A., Cox, C., Gérard, J.-C., 2010. Two-dimensional time-dependent model of the transport of minor species in the Venus night side upper atmosphere. Planet. Space Sci. 58, 1857–1867. http://dx.doi.org/10.1016/j.pss.2010.08.016.

Connes, P., Noxon, J.F., Traub, W.A., Carleton, N.P., 1979. $O_2(^1\Delta)$ emission in the day and night airglow of Venus. Astrophys. J. 233, 29–32.

Counselman, C.C., Gourevitch, S.A., King, R.W., Loriot, G.B., Prinn, R.G., 1979. Venus winds are zonal and retrograde below the clouds. Science 205, 85–87. http://dx.doi.org/10.1126/science.205.4401.85.

Counselman, C.C., Gourevitch, S.A., King, R.W., Loriot, G.B., Ginsberg, E.S., 1980. Zonal and meridional circulation of the lower atmosphere of Venus determined by radio interferometry. J. Geophys. Res. 85, 8026–8030. http://dx.doi.org/10.1029/JA085iA13p08026.

Crisp, D., Meadows, V.S., Bezard, B., deBergh, C., Maillard, J.P., Mills, F.P., 1996. Ground-based near-infrared observations of the Venus nightside: 1.27 μm $O_2(a^1\Delta_g)$ airglow from the upper atmosphere. J. Geophys. Res. 101, 4577–4593. http://dx.doi.org/10.1029/95JE03567.

Drossart, P. et al., 2007. Scientific goals for the observation of Venus by VIRTIS on ESA/Venus Express mission. Planet. Space Sci. 55, 1653–1672. http://dx.doi.org/10.1016/j.pss.2007.01.003.

Gérard, J.C., Cox, C., Saglam, A., Bertaux, J.L., Villard, E., Nehme, C., 2008a. Limb observations of the ultraviolet nitric oxide nightglow with SPICAV on board Venus Express. J. Geophys. Res. 113. http://dx.doi.org/10.1029/2008je003078.

Gérard, J.C. et al., 2008b. Distribution of the O_2 infrared nightglow observed with VIRTIS on board Venus Express. Geophys. Res. Lett. 35. http://dx.doi.org/10.1029/2007gl032021.

Gérard, J.C. et al., 2009a. Concurrent observations of the ultraviolet nitric oxide and infrared O_2 nightglow emissions with Venus Express. J. Geophys. Res. 114. http://dx.doi.org/10.1029/2009je003371.

Gérard, J.C., Saglam, A., Piccioni, G., Drossart, P., Montmessin, F., Bertaux, J.L., 2009b. Atomic oxygen distribution in the Venus mesosphere from observations of O_2 infrared airglow by VIRTIS–Venus Express. Icarus 199, 264–272. http://dx.doi.org/10.1016/j.icarus.2008.09.016.

Gérard, J.C., Soret, L., Piccioni, G., Drossart, P., 2014. Latitudinal structure of the Venus O_2 infrared airglow: A signature of small-scale dynamical processes in the upper atmosphere. Icarus 236, 92–103. http://dx.doi.org/10.1016/j.icarus.2014.03.028.

Hueso, R. et al., 2008. Morphology and dynamics of Venus oxygen airglow from Venus Express/Visible and Infrared Thermal Imaging Spectrometer observations. J. Geophys. Res. 113, E00B02. http://dx.doi.org/10.1029/2008je003081.

Lellouch, E., Clancy, T., Crisp, D., Kliore, A., Titov, D., Bougher, S., 1997. Monitoring of mesospheric structure and dynamics. Venus II, 295–324.

Migliorini, A. et al., 2011. Oxygen airglow emission on Venus and Mars as seen by VIRTIS/VEX and OMEGA/MEX imaging spectrometers. Planet. Space Sci. 59, 981–987. http://dx.doi.org/10.1016/j.pss.2010.05.019.

Moullet, A., Lellouch, E., Moreno, R., Gurwell, M., Sagawa, H., 2012. Wind mapping in Venus' upper mesosphere with the IRAM-Plateau de Bure interferometer. Astron. Astrophys., arXiv:1202.5279.

Ohtsuki, S. et al., 2008. Distributions of the Venus 1.27 μm O_2 airglow and rotational temperature. Planet. Space Sci. 56, 1391–1398. http://dx.doi.org/10.1016/j.pss.2008.05.013.

Piccioni, G. et al., 2009. Near-IR oxygen nightglow observed by VIRTIS in the Venus upper atmosphere. J. Geophys. Res. 114. http://dx.doi.org/10.1029/2008je003133.

Schubert, G. et al., 1980. Structure and circulation of the Venus atmosphere. J. Geophys. Res. 85, 8007–8025. http://dx.doi.org/10.1029/JA085iA13p08007.

Schubert, G. et al., 2007. Venus Atmosphere Dynamics: A Continuing Enigma, Exploring Venus as a Terrestrial Planet. American Geophysical Union, pp. 101–120. doi: http://dx.doi.org/10.1029/176gm07.

Soret, L., Gérard, J.C., Montmessin, F., Piccioni, G., Drossart, P., Bertaux, J.L., 2012a. Atomic oxygen on the Venus nightside: Global distribution deduced from airglow mapping. Icarus 217, 849–855. http://dx.doi.org/10.1016/j.icarus.2011.03.034.

Soret, L., Gérard, J.-C., Piccioni, G., Drossart, P., 2012b. The OH Venus nightglow spectrum: Intensity and vibrational composition from VIRTIS—Venus Express observations. Planet. Space Sci. 73, 387–396. http://dx.doi.org/10.1016/j.pss.2012.07.027.

Sornig, M., Sonnabend, G., Stupar, D., Kroetz, P., Nakagawa, H., Mueller-Wodarg, I., 2013. Venus' upper atmospheric dynamical structure from ground-based observations shortly before and after Venus' inferior conjunction 2009. Icarus 225, 828–839. http://dx.doi.org/10.1016/j.icarus.2012.12.005.

Stewart, A.I.F., Gérard, J.-C., Rush, D.W., Bougher, S.W., 1980. Morphology of the Venus ultraviolet night airglow. J. Geophys. Res. 85, 7861–7870. http://dx.doi.org/10.1029/JA085iA13p07861.

Stiepen, A., Soret, L., Gérard, J.-C., Cox, C., Bertaux, J.L., 2012. The vertical distribution of the Venus NO nightglow: Limb profiles inversion and one-dimensional modeling. Icarus 220, 981–989. http://dx.doi.org/10.1016/j.icarus.2012.06.029.

Stiepen, A., Gérard, J.-C., Dumont, M., Cox, C., Bertaux, J.-L., 2013. Venus nitric oxide nightglow mapping from SPICAV nadir observations. Icarus 226, 428–436. http://dx.doi.org/10.1016/j.icarus.2013.05.031.

Widemann, T., Lellouch, E., Campargue, A., 2007. New wind measurements in Venus' lower mesosphere from visible spectroscopy. Planet. Space Sci. 55, 1741–1756. http://dx.doi.org/10.1016/j.pss.2007.01.005.